CHINESE OPTICS LETTERS

Vol. 21, No. 4 | April 2023

Wavelength-tunable mode-locked fiber laser based on an all-fiber Mach–Zehnder interferometer filter

Fan Yang (杨 凡), Liqiang Zhang (张丽强), Minghong Wang (王明红)*, Nan-Kuang Chen (陈南光), Yicun Yao (姚一村), Zhen Tian (田 振), and Chenglin Bai (白成林)**

School of Physics Science and Information Engineering, Shandong Provincial Key Laboratory of Optical Communication Science and Technology, Liaocheng University, Liaocheng 252000, China

*Corresponding author: wangminghong@lcu.edu.cn

**Corresponding author: baichenglin@lcu.edu.cn

Received June 16, 2022 | Accepted November 25, 2022 | Posted Online April 10, 2023

Wavelength-tunable dissipative solitons and amplifier similaritons have been obtained by inserting all-fiber Mach–Zehnder interferometer (MZI) filters with different free spectral ranges (FSRs) in a Yb-doped mode-locked fiber laser. The MZI filter is fabricated by splicing one segment of seven-core fiber (SCF) between two segments of single-mode fibers. The bandwidth of the filter depends on the FSR of the modulated interference curve and consequently depends on the tapered fiber diameter. Inserting MZI filters with bandwidths in a fiber laser and applying a tensile strain on the tapered SCF, both wavelength-tunable dissipative solitons and amplifier similaritons have been obtained.

Keywords: mode-locked fiber laser; dissipative soliton; amplifier similaritons; Mach–Zehnder interferometer.
DOI: 10.3788/COL202321.041401

1. Introduction

In the past few years, wavelength-tunable pulsed lasers have been in high demand in the fields of biomedical diagnostics[1], laser spectroscopy[2], and optical measurements[3]. Wavelength-tunable lasers can be selected at different wavelengths according to the needs of the actual application area and have such features as low cost, simple structure, and wavelength selectability. The common method of achieving wavelength tunability in fiber lasers is to insert an additional tunable filter device[4–10] in the cavity. Tunable filter units include birefringent plate filters[5], diffraction gratings[6], Lyot filters based on polarization-maintaining fibers[7,8], and Sagnac filters[9]. Among all these devices, birefringent plate filters and diffraction gratings usually complicate the laser cavity owing to the use of discrete elements. The traditional Lyot filter is constructed by inserting one piece of polarization-maintaining fiber between two polarizers, and the channel spacing can be adjusted by changing the birefringent fiber length. However, the filter cannot precisely control the desired central wavelength and repeated channel spacing[11].

On the other hand, with the rapid development of optical fiber manufacturing technology, multicore optical fiber is more and more widely used in interferometers. Mach–Zehnder interferometers (MZIs) based on tapered multicore fiber have been widely used for sensing, such as high temperature sensors[12], precision vibration sensors[13], and strain sensors[14]. The modulated comb interference curves of the multicore fiber-based MZI can be used as filters in fiber lasers. Wavelength-tunable fiber lasers based on MZI filters have been studied and designed with two optical couplers (OCs)[15], and tapered seven-core fiber (SCF)[16] or two-core fiber[17]. Compared with the filters mentioned above, the MZI filters based on tapered multicore fibers have the advantages of simple structure, high reliability, and insensitivity to environmental change. Furthermore, in the MZIs based on tapered multicore fibers, the free spectral range (FSR) could be easily changed by changing the diameter or length of tapered region, which is very useful in normal-dispersion mode-locked fiber lasers. In this type of fiber laser, filters play an important role in shaping the pulse in the spectral domain by cutting the spectrum edges[18]. Depending on the bandwidth of the filter, dissipative solitons or amplifier similaritons could be obtained[19]. So, by inserting MZI filters with different FSRs in the cavity, mode-locked pulses with different evolution mechanisms would be obtained.

In this paper, a normal-dispersion mode-locked fiber laser is demonstrated using a tapered SCF MZI as a comb filter. The MZI is fabricated by splicing a segment of SCF between two segments of single-mode fibers (SMFs). The SCF is weakly coupled and is made into a strongly coupled tapered multicore fiber by heating the fiber with hydrogen. Supermodes are excited and interfere with each other, forming regular modulated interference curves. The FSR of the interference curve depends on the diameter of the tapered region. Stable dissipative solitons

and amplifier solitons have been obtained by inserting the MZI filters with different FSRs in the cavity. The spectra of these two kinds of solitons could both be tuned through stretching the tapered SCF along the horizontal direction.

2. Fabrication of the SCF MZI Filter

The interference filter is fabricated by splicing a segment of SCF between two segments of SMFs. Figure 1(a) shows the cross-sectional view of the SCF. The core diameter is 6.1 μm, and the space between two cores is ~30 μm. Thus, there is no power cross-splicing among these cores, and the SCF is weakly coupled. The numerical apertures (NAs) of the SCF and SMF are 0.2 and 0.14, respectively, and the insertion loss of the SMF-SCF-SMF structure is estimated to be ~1 dB. Using different kinds of fiber to match the NA of SCF and SMF may reduce the loss. The two segments of SMFs are fixed on shift tables by clamps. A hydrogen flame is used to heat the SCF back and forth, while the two shift tables are stretched in the opposite direction. The diameter of the SCF becomes smaller and smaller, and a tapered region is formed. When the incident light is introduced into the tapered part of the SCF through the inner core, the optical field leaks from the inner core into the cladding and the side cores. Due to the circularly symmetric structure of the SCF, two modes are excited by the fundamental mode: the inner-core mode and the side-core supermode[20,21]. The intermodal interference is caused by the optical path difference between these two modes and results in a periodic oscillation curve of the light intensity with wavelength, which is referred to as the interference curve. Figure 1(b) gives the schematic of the fabricated interference filter. The FSR of the interference curve is given by

$$\Delta\lambda = \frac{\lambda^2}{\Delta n_{\text{eff}} \cdot \Delta L}, \tag{1}$$

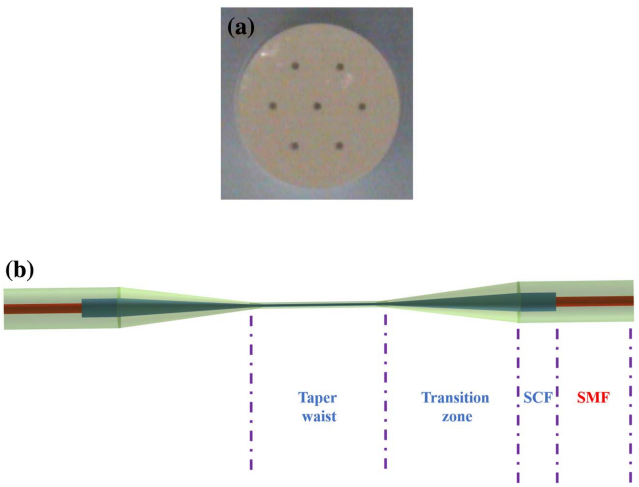

Fig. 1. (a) Schematic diagram of the seven-core fiber; (b) schematic of the MZI filter based on tapered seven-core fiber.

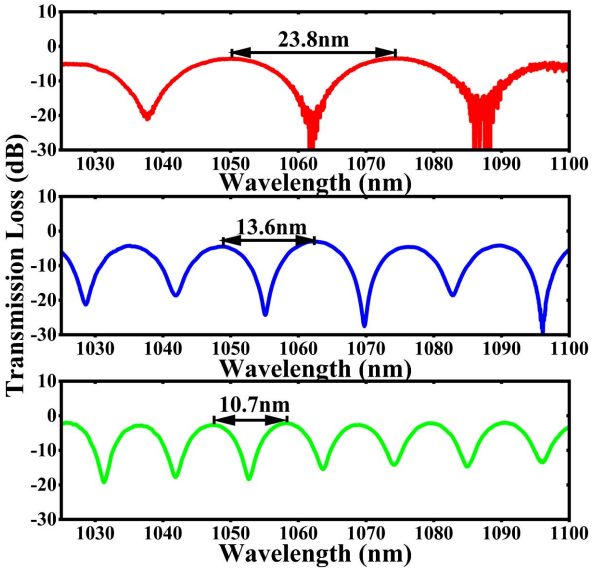

Fig. 2. Transmission spectra of the MZI with different FSRs.

where Δn_{eff} and ΔL denote the effective refractive index difference and physical length difference between the two modes, respectively. The effective refractive index difference increases with the decrease of the tapered diameter and results in a decrease of the FSR. Figure 2 shows the transmission spectra of the MZI with different FSRs. When the diameters of the tapered regions are 12.6, 7.2, and 6.1 μm, the FSRs are 23.8, 13.6, and 10.7 nm, respectively. The insertion loss of the tapered SCF is estimated to be ~3 dB.

3. Experimental Setup

The MZI filter based on a tapered SCF is inserted into a normal-dispersion mode-locked Yb-doped fiber laser in the cavity. The experimental schematic diagram of the fiber laser is presented in Fig. 3. A segment of double-cladding Yb-doped fiber (Liekki Yb1200-10/125) is used as the gain medium, which is pumped by a 976 nm semiconductor laser light through a combiner. The gain fiber has a 10 μm core and 125 μm first-cladding diameter.

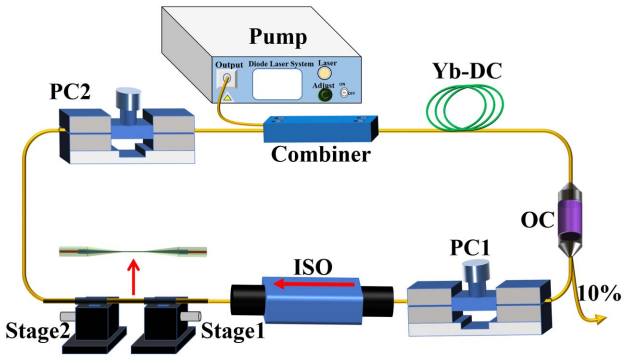

Fig. 3. Schematic diagram of the wavelength-tunable mode-locked fiber laser.

The cladding absorption at 976 nm is 7.4 dB/m. The length of the gain fiber is chosen to be 2 m to absorb most of the pump light. After several times of fusion, the length of the gain fiber remains 1.95 m. A 10/90 OC is used to couple 10% of the optical signal out of the cavity. Two polarization controllers and a polarization-dependent isolator (ISO) are used to realize nonlinear polarization rotation (NPR). The fabricated MZI serves as the spectral filter to reshape the pulse in the spectral domain. The tapered SCF is fixed on two shift stages with UV adhesive, as shown in Fig. 3. Stage 1 is fixed, while Stage 2 can be moved along the horizontal direction. With the moving of Stage 2, the optical path difference between the two modes propagating in the tapered SCF is changed, and the peak wavelengths in the oscillation curve are shifted.

The characteristics of the output pulses are measured by a 15 GHz high-speed photodetector (PD, Newport 818-BB-35), which is linked to a 200 MHz oscilloscope (OSC, GWinstek GDS-2202 E) and a radio-frequency (RF) spectrum analyzer (Keysight N9000B). The spectrum is checked by a spectral analyzer (OSA, Yokogawa AQ 6374) with a resolution of 0.2 nm, and the output pulse duration is measured simultaneously with an autocorrelator (Femtochrome, FR-103XL).

4. Experimental Results and Discussion

An SCF MZI filter with an FSR of 23.8 nm is inserted into the cavity first, and the 3 dB bandwidth of the filter around 1050 nm is estimated to be 12.00 nm. When the pump power reaches 0.6 W, stable mode-locked dissipative solitons can be generated by properly adjusting the two polarization controllers. Figure 4 shows the characteristics of a typical single-wavelength dissipative soliton state when the pump power is set to be 0.8 W. Figure 4(a) gives the spectrum in logarithmic coordinates. The spectrum exhibits steep edges and a square shape, which are the typical characteristics of dissipative solitons[22,23]. The central wavelength and 10 dB bandwidth of the spectrum are 1049.4 and 17.3 nm, respectively. There is a sideband with a central wavelength of 1073.2 nm locating on the right side of the spectrum, which differs from the central wavelength of the spectrum by 23.8 nm. It agrees with the FSR of the MZI filter, indicating the sideband is caused by the periodic filtering effect of the MZI filter. Figure 4(b) shows the pulse sequence recorded by the OSC, showing a repetition rate of 25.5 MHz. Figure 4(c) illustrates the autocorrelation trace. The pulse duration is 11.07 ps, assuming a Gaussian shape. To monitor the stability of the laser, the RF spectrum is measured. Figure 4(d) demonstrates the result with a resolution of 100 Hz in the spectral range from 0 to 300 MHz. The inset presents the RF signal with a resolution of 10 Hz, and the spectral range is from 15.5 to 35.5 MHz. The signal-to-noise ratio is up to 66 dB, which shows that the laser maintains a stable mode-locked state.

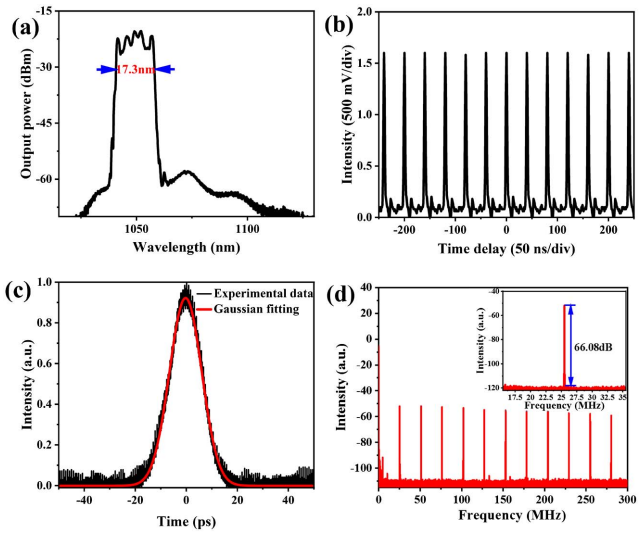

Fig. 4. Characteristics of the dissipative solitons. (a) Optical spectrum; (b) pulse train; (c) autocorrelation trace; (d) RF spectrum.

By applying a tensile strain on the tapered SCF by moving Stage 2, a wavelength tuning range from 1040.08 to 1052.44 nm can be achieved. Figure 5(a) gives the tuning results. The total stretching amount is 0.29 mm. Figure 5(b) shows the variation of pulse duration and spectral bandwidth with the central wavelength. The 10 dB spectral bandwidth varies between 15.9 and 17.6 nm, while the pulse duration ranges from 9.1 to 11.9 ps, respectively. The shortest pulse duration (9.1 ps) is obtained at the central wavelength of 1050.9 nm. Figure 5(c) presents the dependency of pulse energy on the central wavelength of the laser, and the highest pulse energy (2.4 nJ) can be obtained at the central wavelength of 1041.9 nm. It is worth noting that, in the process of stretching the tapered SCF, the output pulse is not stable any more due to the change of polarization state in the laser cavity. It is necessary to adjust the state of the two

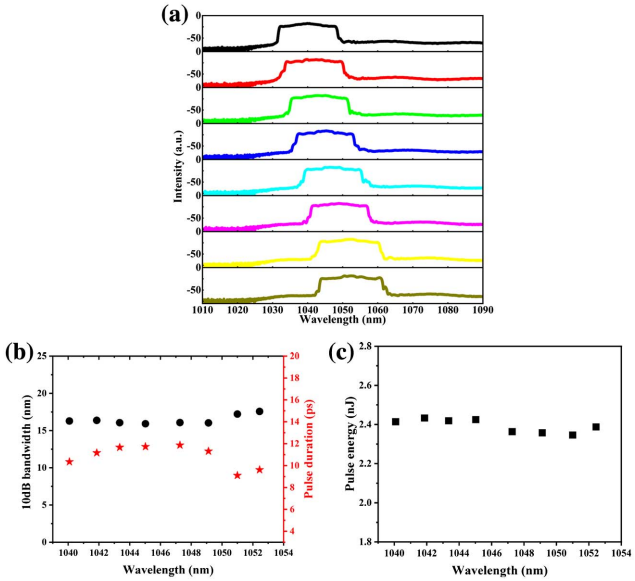

Fig. 5. Tunable results of the dissipative solitons. (a) Optical spectra; (b) variations of 10 dB bandwidth and pulse duration versus the central wavelength; (c) variations of the pulse energy versus the central wavelength.

polarization controllers to make the laser output stable dissipative soliton pulse again.

Benefiting from the comb filtering effect of the interference filter, a switchable dual-wavelength mode-locking state can also be obtained while keeping Stage 2 fixed. The dual-wavelength switching result is obtained through the adjustment of the two polarization controllers. The results are illustrated in Fig. 6. As shown in Figs. 6(b) and 6(c), the central wavelengths are 1049.11 and 1072.91 nm, with 10 dB bandwidths of 17.3 and 17.25 nm, respectively. The wavelength interval is 23.8 nm, which is consistent with the FSR of the filter. Figures 6(d) and 6(e) are the corresponding output pulse train, with a pulse repetition rate of 25.5 MHz. The output pulses are uniformly consistent in the intensity, which confirms the stable mode-locking state of the fiber laser. The autocorrelation traces are given in Figs. 6(f) and 6(g), with pulse durations of 11.46 and 10.35 ps, respectively. The corresponding RF spectra with signal-to-noise ratios of 66.07 and 64.67 dB indicate that the laser works stably and are shown in Figs. 6(h) and 6(i).

Depending on the filter bandwidth used in the cavity, different operation states could be obtained in normal dispersion fiber lasers[6,24]. Generally, with the decrease of the filter bandwidth, the pulse will be switched from dissipative solitons to amplifier similaritons[24]. The FSR of the interference filter is related to the diameter of the tapered region. Filters with different bandwidths could be fabricated conveniently by adjusting the tapering parameters. In our experiment, another MZI filter with a narrow FSR of 13.6 nm is fabricated and inserted into the cavity. The corresponding 3 dB bandwidth of the filter is about 6.64 nm. Amplifier similaritons are obtained when the pump power reaches 1.1 W. Figure 7 reveals the characteristics of a typical single-wavelength amplifier similariton, with the pump power of 1.3 W. Figure 7(a) demonstrates the spectrum. The central wavelength is located at 1067.7 nm, with a 10 dB bandwidth

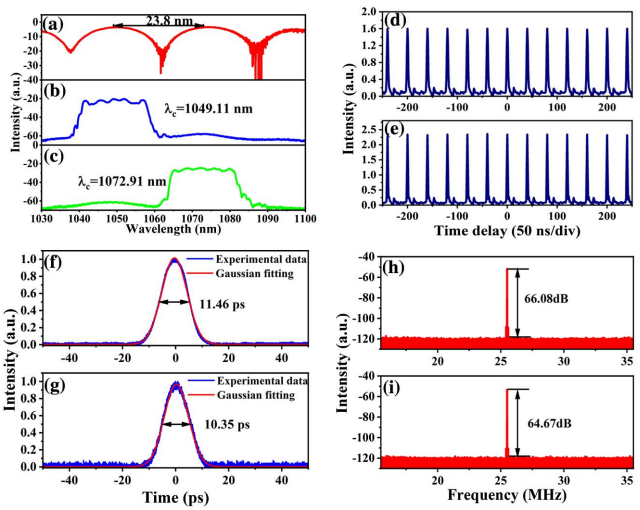

Fig. 6. Switchable dual-wavelength dissipative solitons. (a) Transmission spectrum of MZI filter with an FSR of 23.8 nm; (b), (c) optical spectra; (d), (e) pulse trains; (f), (g) autocorrelation traces; (h), (i) RF spectra.

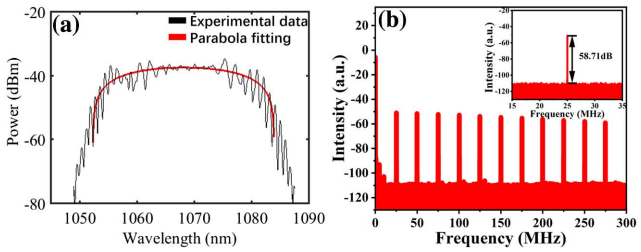

Fig. 7. Characteristics of the amplifier similaritons. (a) Optical spectrum; (b) wide-band RF spectrum up to 300 MHz with a resolution of 100 Hz (inset, the narrow bandwidth RF spectrum from 15.5 to 35.5 MHz).

of 29.9 nm. The pulse duration is measured to be 10.3 ps. Different from the spectrum with steep sides shown in Fig. 4(a), the spectrum agrees with a parabolic fit. A parabolic profile spectrum indicates the generation of amplifier similaritons[25]. Figure 7(b) shows the RF spectrum of the laser recorded by the spectrum analyzer. The RF signal was recorded in the frequency range from 0 to 300 MHz, with a resolution of 100 Hz. The inset in Fig. 7(b) shows the RF signal in the frequency range from 15.5 to 35.5 MHz with a resolution of 10 Hz. The signal-to-noise ratio is 58.71 dB, indicating the laser is operating in a stable state.

Another characteristic of the spectrum shown in Fig. 7(a) is the oscillatory structure. Generally, spectral broadening induced by self-phase modulation (SPM) is accompanied by an oscillatory structure covering the entire frequency range. However, in this kind of spectrum, the oscillations are more serious in the central part of the spectrum[26]. In the spectra observed in our experiment, the oscillations on the edges of the spectrum are more serious than in the central part. Considering the fact that the 10 dB bandwidth of the spectrum is 29.9 nm, and the FSR of the MZI is only 13.6 nm, the sidebands in the spectrum may be attributed to the multiband oscillated transmission curve of the MZI filter.

When the pump power is kept at 1.3 W, the amplifier similaritons keep stable for a long time. By moving the shift Stage 2 in the horizontal direction with a total stretching amount of 0.13 mm, the central wavelength can be tuned from 1052.02 to 1068.16 nm, with a tuning range of 16.14 nm. The tuning results are shown in Fig. 8(a). It can be seen from Fig. 8(b) that the pulse duration varies between 8.5 and 10.3 ps, and the spectral width ranges from 27.6 to 30.2 nm. Figure 8(c) presents the dependency of the pulse energy on the central wavelength. The pulse energy fluctuates between 2.7 and 3.5 nJ. Different from the results of dissipative solitons, the fiber laser maintains a stable mode-locking state during the tuning process, and there is no need to adjust the polarization controllers.

It is worth noting that, in Ref. [27], a nonadiabatic microfiber-based refractive index sensor is reported using a piece of SMF tapered to around 4.61 μm. However, in tapered SMFs, in order to obtain effective interference between the core mode and the cladding mode, a small tapered diameter is needed. Decreasing the tapered diameter induces a high propagating loss, as the light will be scattered on the surface of the tapered waist. For example,

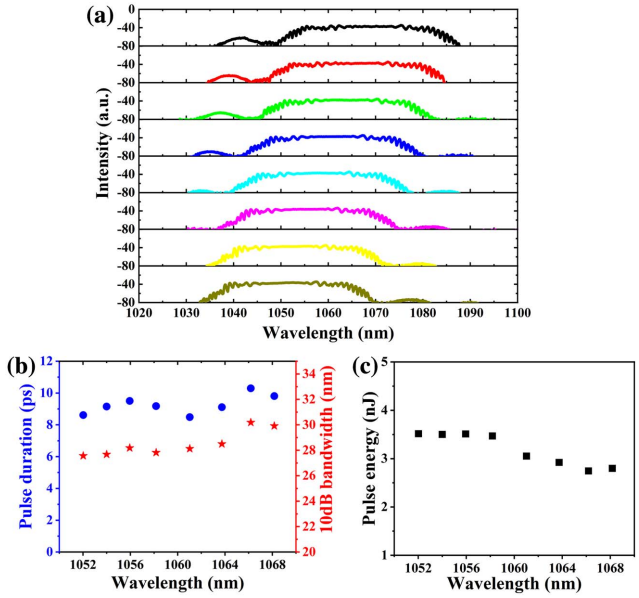

Fig. 8. Tunable results of the amplifier similaritons. (a) Optical spectra; (b) variations of 10 dB bandwidth and pulse duration versus central wavelength; (c) variations of pulse energy versus central wavelength.

when the tapered diameter is chosen to be around 4 μm, higher than 95% light power is coupled out of the tapered fiber[27], resulting in a high transmissivity loss. A gold mirror[28] or another similar taper structure[29] could be used to couple the cladding mode back to the core, and the loss could be decreased greatly. However, adding a gold mirror or another taper complicates the system. Furthermore, in our experiment, the interferometer is used as a filter, and the bandwidth of the filter is related to the FSR. It is more convenient to fabricate an interferometer filter of the desired bandwidth with a tapered SCF, as the FSR decreases continuously during the tapering process, so we could stop tapering immediately once the FSR is close to the target value.

5. Conclusion

In summary, an all-fiber MZI filter has been fabricated by inserting a piece of tapered SCF between two pieces of SMFs. Compared with other kinds of filters, the proposed MZI filter has the advantages of low cost, easy fabrication, all-fiber structures, and low transmission loss. When the filter is used for spectrum shaping in mode-locked fiber lasers, the most arresting feature is the easily available desired bandwidth. In our experiment, using the MZIs with different FSRs as the filters, stable dissipative solitons and amplifier similaritons have been obtained in a Yb-doped fiber laser mode-locked by NPR. Both of these two kinds of pulses can be tuned by stretching the tapered SCF along the horizontal direction. The central wavelength of dissipative solitons can be tuned from 1040.08 to 1052.44 nm, while the tuning range of the amplifier similaritons is 1052.02 to 1068.16 nm. This pulsed Yb-doped fiber laser based on MZI filter may have applications in biomedical diagnostics, laser spectroscopy, optical measurements, and other fields.

Acknowledgement

This work was supported in part by the National Natural Science Foundation of China (No. 61875247), the Natural Science Foundation of Shandong Province (Nos. ZR2020QF086 and ZR2022MF253), and Liaocheng University (Nos. 318052199, 318012023, 318051412, 31805180101, 319190301, and 318051411).

References

1. J. Q. Lin, Z. P. Dong, T. H. Dong, Y. M. Zhang, C. S. Dai, P. J. Yao, C. Gu, and L. X. Xu, "All-fiber figure-eight wavelength-tunable noise-like pulse lasers," Opt. Laser Technol. **141**, 107146 (2021).
2. Z. H. Tao, X. Li, W. Z. Ma, X. B. Ding, T. S. Wang, H. L. Jiang, Y. B. Wang, and Y. Lou, "All-fiber 2.1 μm band tunable continuous-wave and soliton mode-locked Ho-doped fiber laser," Opt. Commun. **515**, 128157 (2022).
3. K. Zhao, W. Yan, M. L. Liu, L. S. Wang, H. X. Li, M. S. Zhang, Z. Q. Jia, R. Z. Zhai, and M. Z. Liu, "Tunable ytterbium fiber laser mode-locked with a nonlinear amplifying loop mirror," Opt. Laser Technol. **148**, 107764 (2022).
4. M. Schultz, H. Karow, D. Wandt, U. Morgner, and D. Kracht, "Ytterbium femtosecond fiber laser without dispersion compensation tunable from 1015 nm to 1050 nm," Opt. Commun. **282**, 2567 (2009).
5. K. Tamura, C. R. Doerr, H. A. Haus, and E. P. Ippen, "Soliton fiber ring laser stabilization and tuning with a broad intracavity filter," IEEE Photon. Technol. Lett. **6**, 697 (1994).
6. C. Ma, A. Khanolkar, and A. Chong, "High-performance tunable, self-similar fiber laser," Opt. Lett. **44**, 1234 (2019).
7. Y. Li, J. J. Tian, M. R. Quan, and Y. Yao, "Tunable multiwavelength Er-doped fiber laser with a two-stage Lyot filter and intensity-dependent loss," IEEE Photon. Technol. Lett. **29**, 287 (2017).
8. X. Luo, T. H. Tuan, T. S. Saini, H. P. T. Nguyen, T. Suzuki, and Y. Ohishi, "Tunable and switchable all-fiber dual-wavelength mode locked laser based on Lyot filtering effect," Opt. Express **27**, 14635 (2019).
9. T. S. Wang, X. F. Miao, X. F. Zhou, and S. Qian, "Tunable multiwavelength fiber laser based on a double Sagnac HiBi fiber loop," Appl. Opt. **51**, C111 (2012).
10. S. Ma, B. Zhang, Q. He, J. Guo, and Z. Jiao, "Wavelength-tunable mode-locked Yb-doped fiber laser based on nonlinear Kerr beam clean-up effect," Chin. Opt. Lett. **20**, 041403 (2022).
11. M. M. Han, X. L. Li, S. M. Zhang, H. Y. Han, J. M. Liu, and Z. J. Yang, "Tunable and channel spacing precisely controlled comb filters based on the fused taper technology," Opt. Express **26**, 265 (2018).
12. S. Zhou, B. Huang, and X. W. Shu, "A multi-core fiber based interferometer for high temperature sensing," Meas. Sci. Technol. **28**, 045107 (2017).
13. J. Villatoro, E. Antonio-Lopez, J. Zubia, A. Schülzgen, and R. Amezcua-Correa, "Interferometer based on strongly coupled multi-core optical fiber for accurate vibration sensing," Opt. Express **25**, 25734 (2017).
14. L. Gan, R. X. Wang, M. Tang, L. Duan, B. R. Li, S. N. Fu, W. J. Tong, H. F. Wei, D. M. Liu, and P. P. Shum, "Space-division multiplexed multicore fiber Mach-Zehnder interferometer for joint temperature and strain sensing," in *Optical Fiber Communications Conference and Exhibition (2016)*, paper W2A.35.
15. Q. Zhao, L. Pei, Z. Ruan, J. Zheng, J. Wang, M. Tang, J. Li, and T. Ning, "Tunable and wavelength interval precisely controlled erbium-doped fiber laser by employing the fused taper technology," Chin. Opt. Lett. **20**, 011402 (2022).
16. L. Q. Zhang, Z. Tian, N. K. Chen, H. L. Han, C. N. Liu, K. T. V. Grattan, B. M. A. Rahman, H. M. Zhou, S. K. Liaw, and C. L. Bai, "Room-temperature power-stabilized narrow-linewidth tunable erbium-doped fiber ring laser

based on cascaded Mach-Zehnder interferometers with different free spectral range for strain sensing," J. Light. Technol. **38**, 1966 (2020).
17. Z. J. Tang, S. Q. Lou, and X. Wang, "Stable and widely tunable single-/dual-wavelength erbium-doped fiber laser by cascading a twin-core photonic crystal fiber based filter with Mach-Zehnder interferometer," Opt. Laser Technol. **109**, 249 (2019).
18. A. Chong, J. Buckley, W. Renninger, and F. Wise, "All-normal-dispersion femtosecond fiber laser," Opt. Express **14**, 10095 (2006).
19. L. Q. Zhang, Z. Zhuo, N. K. Chen, Z. Tian, and Y. R. Xie, "Wave plate-dependent lasing regimes transitions in an all-normal-dispersion fiber laser mode-locked by nonlinear polarization rotation," Opt. Laser Technol. **126**, 106085 (2020).
20. D. Yan, Z. Tian, N. K. Chen, L. Zhang, Y. Yao, Y. Xie, P. P. Shum, K. T. V. Grattan, and D. Wang, "Observation of split evanescent field distributions in tapered multicore fibers for multiline nanoparticle trapping and microsensing," Opt. Express **29**, 9532 (2021).
21. M. S. Yoon, S. B. Lee, and Y. G. Han, "In-line interferometer based on intermodal coupling of a multicore fiber," Opt. Express **23**, 18316 (2015).
22. H. Chen, S. P. Chen, Z. F. Jiang, and J. Hou, "80 nJ ultrafast dissipative soliton generation in dumbbell-shaped mode-locked fiber laser," Opt. Lett. **41**, 4210 (2016).
23. J. L. Luo, Y. Q. Ge, D. Y. Tang, S. M. Zhang, D. Y. Shen, and L. M. Zhao, "Mechanism of spectrum moving, narrowing, broadening, and wavelength switching of dissipative solitons in all-normal-dispersion Yb-fiber lasers," IEEE Photonics J. **6**, 1500608 (2014).
24. Y. Q. Du and X. W. Shu, "Transformation from conventional dissipative solitons to amplifier similaritons in all-normal dispersion mode-locked fiber lasers," IEEE Photonics J. **10**, 1500911 (2018).
25. J. K. Shi, L. Chai, X. W. Zhao, B. W. Liu, M. L. Hu, Y. F. Li, and C. Y. Wang, "95 nJ dispersion-mapped amplifier similariton fiber laser at 8.6 MHz repetition rate with linear cavity configuration," Opt. Express **23**, 18330 (2015).
26. G. P. Agrawal, *Nonlinear Fiber Optics* (Elsevier, 2013).
27. W. B. Ji, H. H. Liu, S. C. Tjin, K. K. Chow, and A. Lim, "Ultrahigh sensitivity refractive index sensor based on optical microfiber," IEEE Photon. Tech. Lett. **24**, 1872 (2012).
28. Z. Tian, S. S.-H. Yam, and H. P. Loock, "Refractive index sensor based on an abrupt taper Michelson interferometer in a single-mode fiber," Opt. Lett. **33**, 1105 (2008).
29. P. Lu, L. Men, K. Sooley, and Q. Chen, "Tapered fiber Mach-Zehnder interferometer for simultaneous measurement of refractive index and temperature," Appl. Phys. Lett. **94**, 131110 (2009).